



# Silver-integrated EDM processing of TiAl6V4 implant material has antibacterial capacity while optimizing osseointegration

Hilmar Büsselmeier<sup>a,1</sup>, Ann-Kathrin Meinshausen<sup>a,1</sup>, Viet Duc Bui<sup>b</sup>, Joachim Döring<sup>a</sup>, Vadym Voropai<sup>a</sup>, Adrian Buchholz<sup>a</sup>, Andreas J. Mueller<sup>c,d</sup>, Karsten Harnisch<sup>e</sup>, André Martin<sup>b</sup>, Thomas Berger<sup>b</sup>, Andreas Schubert<sup>b,f</sup>, Jessica Bertrand<sup>a,d,\*</sup>

<sup>a</sup> Department of Orthopaedic Surgery, Otto-von-Guericke University Magdeburg, Germany

<sup>b</sup> Professorship Micromanufacturing Technology, Chemnitz University of Technology, Chemnitz, Germany

<sup>c</sup> Institute of Molecular and Clinical Immunology, Otto-von-Guericke University Magdeburg, Germany

<sup>d</sup> Health Campus Immunology, Infectiology and Inflammation, Otto-von-Guericke University Magdeburg, Magdeburg, Germany

<sup>e</sup> Institute of Materials and Joining Technology, Otto-von-Guericke University, Magdeburg, Germany

<sup>f</sup> Fraunhofer Institute for Machine Tools and Forming Technology, Chemnitz, Germany

## ABSTRACT

Periprosthetic joint infections (PJI) are a common reason for orthopedic revision surgeries. It has been shown that the silver surface modification of a titanium alloy (Ti–6Al–4V) by PMEDM (powder mixed electrical discharge machining) exhibits an antibacterial effect on *Staphylococcus* spp. adhesion. Whether the thickness of the silver-modified surface influences the adhesion and proliferation of bacteria as well as the ossification processes and *in-vivo* antibacterial capacity has not been investigated before. Therefore, the aim of this work is to investigate the antibacterial effect as well as the *in vitro* ossification process depending on the thickness of PMEDM silver modified surfaces.

The attachment of *S. aureus* on the PMEDM modified surfaces was significantly lower than on comparative control samples, independently of the tested surface properties. Bacterial proliferation, however, was not affected by the silver content in the surface layer. We observed a long-term effect of antibacterial capacity *in vitro*, as well as *in vivo*. An induction of ROS, as indicator for oxidative stress, was observed in the bacteria, but not in osteoblast-like cells. No influence on the *in vitro* osteoblast function was observed, whereas osteoclast formation was drastically reduced on the silver surface. No changes in cell death, the metabolic activity and oxidative stress was measured in osteoblasts.

We show that already small amounts of silver exhibit a significant antibacterial capacity while not influencing the osteoblast function. Therefore, PMEDM using silver nano-powder admixed to the dielectric represents a promising technology to shape and concurrently modify implant surfaces to reduce infections while at the same time optimizing bone ingrowth of endoprosthesis.

## 1. Introduction

Besides the aseptic loosening and malpositioning of an orthopedic implant, the periprosthetic joint infection (PJI) is a common reason for revision surgery [1]. The infection rate is about 1% for hip and about 2% for knee endoprosthesis after primary implantation [2]. After a previous PJI revision surgery, the risk of re-infection increases up to 10% [3–5]. PJI usually occurs in the first two years (60–70%) after joint replacement [6,7].

The classification of PJIs is divided into acute, subacute, and late infections, which mainly depends on the pathogen causing the PJI. *Staphylococcus aureus* is, because of its high virulence, a frequently

detected pathogen in acute PJI. An acute PJI is defined as an infection up to 3 months after the endoprosthesis implantation. Both subacute (3–12 months post-surgical) and late (12–48 months post-surgical) infections are caused by less virulent pathogens. Here, coagulase-negative *staphylococci* or *enterococci* are often detected in these cases [7]. However, late infections can also be caused by a hematogenous infection, where the bacteria are transported via the bloodstream from different areas of the body to the implant. Again, a typical pathogen of late-stage PJI with a hematogenous origin is *S. aureus* [8]. *S. aureus* and *S. epidermidis* are the most common bacteria associated with bone infections caused by titanium implants [9].

To keep the risk of infections low, antibiotics are given during and

Peer review under responsibility of KeAi Communications Co., Ltd.

\* Corresponding author. Department of Orthopaedic Surgery, Otto-von-Guericke University, Leipziger Straße 44, D-39120, Magdeburg, Germany.

E-mail address: [Jessica.bertrand@med.ovgu.de](mailto:Jessica.bertrand@med.ovgu.de) (J. Bertrand).

<sup>1</sup> Both authors contribute equally.

<https://doi.org/10.1016/j.bioactmat.2023.08.019>

Received 22 September 2022; Received in revised form 29 April 2023; Accepted 24 August 2023

2452-199X/© 2023 The Authors. Publishing services by Elsevier B.V. on behalf of KeAi Communications Co. Ltd. This is an open access article under the CC BY-NC-ND license (<http://creativecommons.org/licenses/by-nc-nd/4.0/>).

after the surgery to prevent a PJI. However, antibiotics mainly affect the PJIs occurring during the immediate post-implantation time [10]. Especially, hematogenous or late infections cannot be prevented by antibiotic therapy during and post-surgery. The use of antibacterial coatings on implants, with the aim to interfere with the bacterial adhesion on the implants, therefore, represents a promising antibacterial strategy to prevent PJI [11,12]. Antibacterial coatings based on silver or copper showed a high efficiency against GRAM-positive and GRAM-negative bacteria [12–16]. It has been shown *in vitro* and *in vivo* that silver-coated implants can reduce the number of infections, even in cases of revision surgery due to previous PJI [17]. Silver ions used for current antibacterial implant coatings are rapidly released from the surface within the first hours after surgery, influencing mainly early infection rates [18]. However, most approaches currently are based on silver nanoparticles to induce bone repair especially for PJI revision surgeries [19–22].

A variety of technologies such as physical vapor deposition, chemical vapor deposition, ion implantation and thermal spraying have been used to apply potential antibacterial surface modifications. The novelty of this manuscript is, that we apply Electrical Discharge Machining (EDM) for the generation of a silver modified surface layer, that includes silver within the implant material surface layer. EDM is a nonconventional process that is widely used for machining various metallic materials of medical devices [23]. By adding silver nano-powders to the dielectric fluid, the EDM process has been developed to powder mixed electrical discharge machining (PMEDM), and has been used for machining the implant and concurrent transfer of silver to the modified layer of Ti–6Al–4V implant materials thereby creating antibacterial properties [24].

The antibacterial capacity of silver ions is based on different mechanisms that potentially contribute to the antibacterial capacity [25]. Silver ions bind to sulfhydryl groups and proteins present in the bacterial membrane, which gets destabilized by a progressive release of lipopolysaccharides [26,27]. After entering the cell, the silver ions interact with the thiol group of proteins leading to an inhibition of metabolic pathways [28–30]. The inhibition increases the reactive oxygen species (ROS), resulting in oxidative stress, protein damage, DNA strand breaks, and cell death [30,31]. It has already been shown that even low silver concentrations decrease the adhesion of bacteria to a surface [17,24], but cannot prevent biofilm formation completely [24,32]. However, besides silver exhibiting a marked antibacterial activity, potential toxic effects on eukaryotic cells should be taken into account. Some studies show that silver ions can cross the cytoplasmic membrane and interact with DNA or induce oxidative damage or interfere with the cell cycle [33,34]. Further studies need to be performed to establish the optimal dose-response spectrum for antibacterial property of potential implant surface modifications, whilst exhibiting optimal osseointegrative capacity [20].

Therefore, the aim of this work is to investigate the antibacterial effect as well as ossification processes of PMEDM modified Ti–6Al–4V surfaces integrated with silver.

## 2. Materials and methods

### 2.1. Powder mixed electrical discharge machining (PMEDM)

The principle of the PMEDM surface modification is shown in Fig. 1. In the plasma channel of the discharge, temperatures over  $T = 10,000$  K prevail locally, which leads to melting and evaporation of the tool electrode and work piece materials as well as silver powder particles admixed in the dielectric fluid. After the re-solidification process, the modified layer, formed by a series of overlapping craters, contains combined materials from the work piece, tool electrode and silver. Silver is transferred to the modified layer through the four mechanisms implantation, alloying, attachment and spattering as represented in Fig. 1 [26].

During PMEDM, the distribution of silver powder in the machining gap plays a vital role in the distribution of silver deposited in the modified surface. The use of cylindrical tool electrodes with side flushing results in non-uniform distribution of the deposited silver, whereby the silver contents tends to decrease from the outer edge to the center of the modified surface. This is due to the un-uniformity of silver powder distribution and flushing conditions in the machining gap [27]. This negative effect could be reduced by utilizing sheet tool electrodes without rotation in this study. Before machining, the work piece surfaces and tips of the tool electrodes were ground and then polished to achieve a flat surface and a roughness value of  $1 \mu\text{m} R_z$ .

The samples had a size of  $(10 \times 10 \times 1) \text{mm}^3$ . For antibacterial and osseointegrative investigations three areas each with a size of  $(3 \times 4) \text{mm}^2$  were modified on each plate. Experimental conditions and

**Table 1**  
PMEDM experimental conditions and parameters.

Machine	Sarix T1-T4 $\mu$ -EDM machine
Work piece	- Material: Ti–6Al–4V - Size: 10 mm $\times$ 10 mm $\times$ 1 mm
Tool electrode	- Material: Ti–6Al–4V - Sheet electrodes, sizes (W $\times$ H): 3 mm $\times$ 1 mm 12 mm $\times$ 1 mm
Dielectric fluid	HEDMA111
Powder added to dielectric	- Material: Silver 99.9% - Particle size: (50 ... 60) nm - Concentrations: 15 g/l, 17.5 g/l and 20 g/l
Discharge energies	10 $\mu\text{J}$ , 55 $\mu\text{J}$ and 125 $\mu\text{J}$
Polarity	Positive at tool electrode

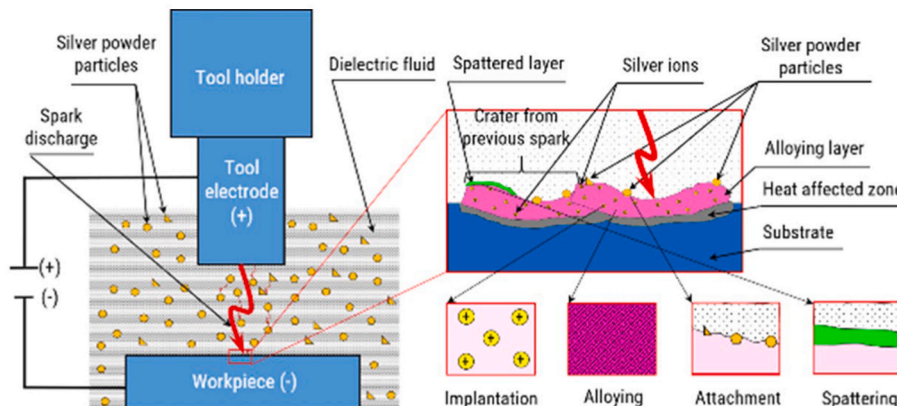


**Fig. 1.** Principle of the PMEDM surface modification [26].

parameters of the PMEDM process are shown in Table 1.

## 2.2. Surface characterization

Each sample was cleaned in an ultrasonic bath filled with ethanol at room temperature for 10 min, and then air dried. The surface topography and composition was analyzed using a scanning electron microscope (SEM) and energy dispersive X-Ray spectroscopy (EDS) (Thermo Fisher Scientific, Waltham, MA), as well as a ZEISS EVO MA 10 (Carl Zeiss Microscopy GmbH, Jena, Germany). The roughness was measured using a  $\mu$ surf expert confocal microscope (NanoFocus AG, Oberhausen, Germany). The measuring field of  $1280 \mu\text{m} \times 320 \mu\text{m}$  was acquired with a 50x magnification objective offering a lateral resolution of 267 nm and a vertical resolution of 4 nm. Roughness parameters according to DIN EN ISO 25178-2 such as the arithmetic average roughness (Sa) and average maximum profile height (Sz) were measured.

The mechanical properties of the modified layer were investigated using nano-indentation experiments according to DIN EN ISO 14577-1/-4 (NHT3 from Anton Paar GmbH, Graz, Austria). A Berkovich diamond indenter with a centerline-to-face angle of  $65.3^\circ \pm 0.3^\circ$  was used to evaluate the hardness and indentation modulus of the coatings. Quasi-static load-controlled measurements were performed with a constant load increasing rate of 24 mN/min to a maximum of 12 mN. In order to minimize substrate effects, the maximum indentation depth was kept to less than 10% of the layer thickness.

For evaluation of depth dependent hardness, a dynamic mechanical analysis (DMA) was performed by nano-indentation tests ( $n = 6$ ) in sinus mode. During the measurement the indentation force is increased up to 500 mN with a constant load rate of 300 mN/min according to sinus function and a frequency of 5 Hz as well as an amplitude of 50 mN.

The thickness of the modified layer was analyzed on cross-section samples. The samples were carefully ground, polished with a wet abrasive paper and afterwards chemically etched using Kroll solution. The cross-sectional shape of each sample was scanned using a Keyence VK9700 confocal 3D laser scanning microscope and analyzed with Keyence VK-analyser software. Fifty points per sample were analyzed, thus allowing for a calculation of an average thickness as well as standard deviation.

## 2.3. SEM and EDS analyses

SEM and EDS surface area analyses were performed using a FEI Scios DualBeam (Thermo Fisher Scientific, Waltham, MA). Integral EDS analyses of the surface area were conducted at a magnification of 200x at 10 kV using a TEAM Trident System (EDAX, AMETEK GmbH, Weiterstadt, Germany). Elemental mappings were collected at a magnification of 10,000x at 20 kV.

## 2.4. Scratch tests

The hardness of the surface layer was examined with a scratch test according to DIN EN ISO 20502 (Table 2). A Micro Scratch Tester (MST3 Anton Paar TriTec SA, Peseux, Switzerland) was used.

**Table 2**  
Scratch tests parameters.

	linear Scratch
starting force [N]	0.03
end force [N]	10 (15)
loading rate [N/min]	99.65
scratch speed [mm/min]	4.99
scratch path [mm]	1 (1.5)
radius Rockwell diamond [ $\mu\text{m}$ ]	100

## 2.5. Cultivation with *Staphylococcus aureus* eGFP/mKikumeGR

The staphylococcal strains *SH1000/pSB2035* and *SH1000/pMD303* (both from AG Müller, IMKI University Hospital Magdeburg) were cultured as an overnight culture in Brain heart infusion (BHI) medium at  $37^\circ\text{C}$  and 150 rpm. A bacterial solution with an OD 1 was inoculated from this overnight culture. The PMEDM silver-coated samples were inoculated 1:1000 with bacteria from the overnight culture in 1 ml BHI medium. After incubation at  $37^\circ\text{C}$  for 24h, the samples were washed twice with PBS and then inoculated with 1 ml of new BHI medium. This was followed by another incubation for 24h at the above conditions. The *SH1000/pSB2035* samples were washed twice with PBS (Dulbecco) before and after fixation with 4% formaldehyde.

## 2.6. Cultivation with *Staphylococcus aureus*/eGFP

The *Staphylococcus aureus* strain *SH1000/pSB2035* was cultivated and fixed on the PMEDM modified sample platelets according to the above-mentioned procedure. Due to the plasmid, encoding for the green fluorescent protein eGFP, the bacteria were visualized under the fluorescence microscope (Axio Observer, Carl Zeiss, Jena, Germany). 5 images were taken per sample and the arithmetic mean values were calculated for these. The area of green fluorescence was measured using Image J.

## 2.7. Cultivation of *Staphylococcus capitis* and long term antibacterial tests

*Staphylococcus capitis* was cultured as an overnight culture in tryptic soy broth (TSB) medium at  $37^\circ\text{C}$  and 150 rpm. A bacterial solution with an OD 1 was inoculated from this overnight culture. The PMEDM silver-coated samples were inoculated 1:10.000 with bacteria from the overnight culture in 1 ml TSB medium. After incubation at  $37^\circ\text{C}$  for 24h, the samples were washed twice with PBS and then inoculated with 1 ml of new TSB medium. The medium was changed every second day. This was followed by another incubation for 7 days at the above conditions. The samples were washed twice with PBS (Dulbecco) before and after fixation with 4% formaldehyde. The bacteria were stained with DAPI to visualize the adhering bacteria using a fluorescence microscope (Axio Observer, Carl Zeiss, Jena, Germany). 5 images were taken per sample and the arithmetic mean values were calculated for these. The area of green fluorescence was measured using Image J.

## 2.8. Cultivation with mKikumeGR proliferation assay

The *Staphylococcus aureus* strain *SH1000/pMD303* (AG Müller, IMKI Uniklinikum Magdeburg) is transformed with a plasmid encoding for the green fluorescent protein mKikumeGr. The bacteria were cultivated according to the scheme described above. The mKikumeGr protein can be converted into a red fluorescent protein by 30 s photoconversion at a wavelength of 405 nm by a  $2 \times 2$  LED diode [26]. The red fluorescent protein begins to gradually be diluted after photoconversion during proliferation, as proliferating bacteria can only express green fluorescent mKikumeGr protein. Therefore, the proliferation rate can be determined from the ratio of the red and green fluorescent bacteria. After this photoconversion, the sample platelets were incubated in BHI medium for 60 min at  $37^\circ\text{C}$  to allow for proliferation. Subsequently, the sample platelets were fixed with 4% formaldehyde for 30 min and washed with PBS. Images were acquired using a fluorescence microscope (Axio Observer, Carl Zeiss, Jena, Germany) using the 488 nm and 555 nm filter set. The combined red and green channel was taken for analysis and the Fiji program in ImageJ was used.

## 2.9. TUNEL staining for cell death

To test the cell death influenced by silver, SaOs-2 cells were seeded

on the silver surfaces. For this purpose, Ti–6Al–4V sample surfaces without PMEDM modification (control TAV surfaces) were used as well as coverslips for the positive and negative control. In order to keep the cells and the solutions of the kit on the surface, the surfaces were rimmed with sterile petroleum jelly. However, the cells were seeded with a cell number of  $1 \times 10^5$  in a 24 well plate on the sample plates. For culturing RPMI medium with the addition of 10% FCS and 1% P/S was used. The cells were incubated for 24 h on the surfaces. The medium supernatant was removed from the platelet, and washed twice with 1x PBS. For staining the *in situ* cell death kit from Roche was used. Approximately 80  $\mu$ l of TUNEL reagent was added to the surface of the platelets. For the positive control, the cells were previously stimulated with DNase. The reagent was incubated for 1h at 37 °C in the dark. Subsequently, the platelets were washed twice with 1x PBS and fixed for 15 min at RT with formaldehyde, again the platelets were washed twice with 1x PBS. Followed by staining with DAPI (1:1000) and Phalloidin (1:100) in PBS. The images were taken using a fluorescence microscope (Axio Observer, Carl Zeiss, Jena, Germany).

### 2.10. WST staining for cell viability

To test the cell viability, SaOs-2 cells were seeded on the silver surfaces, as a control TAV surfaces and glass coverslips were used. In order to keep the cells and the solutions of the kit on the surface, the surfaces were rimmed with sterile petroleum jelly. However, the cells were seeded with a cell number of  $1 \times 10^5$  in a 24 well plate on the sample plates. For culturing RPMI medium with the addition of 10% FCS and 1% P/S was used. The cells were incubated for 24 h on the surfaces. For the WST assay the assay Kit from Abcam was used. For staining, 10 ml of WST reagent was added to the platelets and mixed with the medium. This was followed by incubation for 3h at 37°. For measurement, 100  $\mu$ l of the supernatant was transferred to a new well plate and the absorbance was measured via Tecan at 430 nm.

### 2.11. DHE assay for investigation of reactive oxygen species

To investigate the reactive oxygen species the DHE assay Kit from Abcam was used. For the analyzation, the SaOs-2 cells were seeded on the silver surfaces, as a control TAV surfaces were used as well as coverslips for the positive and negative control. In order to keep the cells and the solutions of the kit on the surface, the surfaces were rimmed with sterile petroleum jelly. However, the cells were seeded with a cell number of  $0.3 \times 10^5$  in a 24 well plate on the sample plates. For culturing RPMI medium with the addition of 10% FCS and 1% P/S was used. The cells were incubated for 24 h on the surfaces. The reagent were prepared as described in the Kit. The Antimycin A was used as positive control, while *N*-acetyl Cysteine was used for the negative control. For staining, the medium was removed from the surface and washed with 80  $\mu$ l of Cell-Based Buffer. Subsequently, 60  $\mu$ l of the buffer was removed and 60  $\mu$ l of the ROS staining solution was added. Additional, 8  $\mu$ l of *N*-acetyl cysteine was added for preparing the negative control. The incubation was for 30 min at 37°degrees. For the positive control, 10  $\mu$ l Antimycin A was added and all samples were again incubated for 1h at 37°. After incubation, all platelets were washed with 100  $\mu$ l Cell based Assay buffer. The sample plates were fixed with formaldehyde. Followed by staining with DAPI. The images were taken using a fluorescence microscope (Axio Observer, Carl Zeiss, Jena, Germany).

### 2.12. ROX assay for investigation of the reactive oxygen species in *Staphylococcus capitis*

To measure the reactive oxygen species in *Staphylococcus*, the *S. capitis* DSM 20326 was used. The bacteria were incubated overnight at 37 °C and 150 rpm in TSB from a glycerol stock. After OD determination of 600 nm a culture with an OD of 1 was prepared. The silver platelets, TAV platelets and glass coverslips were inoculated in 1:100 in TSB

medium, with an end Volume of 1 ml. The samples were incubated at 37 °C for 24h and washed twice with PBS. For the positive control the glass coverslips were incubated with 0.05% H<sub>2</sub>O<sub>2</sub> for 2 min. For the staining the CellROX Oxidative Stress Kit deep red was used from ThermoFisher. In order to keep the solution of the kit on the surface, the surfaces were rimmed with sterile petroleum jelly. For the staining the CellROX reagent with a final concentration of 5  $\mu$ M was added to the surfaces and incubated for 30 min at 37 °C. The cells were washed 3 times with 1x PBS and fixed with formaldehyde. Followed by staining with DAPI. The images were taken using a fluorescence microscope (Axio Observer, Carl Zeiss, Jena, Germany).

### 2.13. Osteogenic differentiation and alizarin red S assay

SaOs-2 cells or bone marrow macrophages (BMM) from wildtype were differentiated into osteoblasts. The SaOs-2 cells from human osteosarcoma cells were seeded with a cell number of  $0.5 \times 10^5$  in a 24 well plate on the sample plates.  $3 \times 10^5$  BMMs were seeded after isolation from murine femur and tibia bones with a cell count of cells. Cells were then treated with osteogenic medium (DMEM 0.2 mM ascorbic acid, 10 mM glycerol phosphate, 10 nM dexamethasone) for 10 days. The medium was renewed three times per week. After discarding the medium, cells were fixed with 4% PFA for 30 min and washed with distilled water (dH<sub>2</sub>O). Staining was performed with Alizarin Red S solution (2g Alizarin Red S (Sigma-Aldrich, St. Louis, MO, USA) in 100 ml dH<sub>2</sub>O at pH 4) for 45 min. De-staining was performed with 50  $\mu$ l cetylpyridium chloride (Sigma-Aldrich, St. Louis, MO, USA). After 5–10 min incubation time, the solution was transferred to a 96-well microplate and the absorbance was measured at 540 nm (Infinite F200 Pro, Tecan Group AG, Maennedorf, Switzerland).

### 2.14. In vitro osteoclast differentiation

For in-vitro osteoclast formation, we used bone marrow-derived macrophages (BMMs) as described before [35]. Briefly, bone marrow cells were cultured in  $\alpha$ -MEM containing 10% fetal calf serum (Invitrogen) and 50 ng/ml M-CSF (R&D) for 3 days to obtain BMM's. BMM's were cultured with 50 ng/ml M-CSF and 50 ng/ml RANKL (R&D). Medium was changed on day 4. On day 11, osteoclast-like cells were characterized by DAPI and Phalloidin staining. We counted the number of three or more DAPI-positive multinucleated cells.

#### 2.14.1. RNA extraction, cDNA synthesis, real-time RT-PCR

Total RNA was extracted from differentiated osteoclasts using TRIzol reagent (Invitrogen). 1 ng of total RNA from each sample was reverse transcribed using High-Capacity cDNA Reverse Transcription Kit (Applied Biosystems) using oligo dT primers. Quantitative polymerase chain reaction (PCR) was performed with SYBR Green I (SG) asymmetrical cyanine dye (SYBR) green using Applied Biosystems™ PRISM 7900HT (Thermo Scientific). Absolute quantification was carried out using standard curves. Target gene expression was normalized to Glyceraldehyde-3-Phosphate Dehydrogenase (GAPDH). The following primers were used: TRAP (forward CGACCATTGTTAGCCACATACG and reverse TCGTCTGA AGATACTGCAGGTT), Cathepsin K (forward GGAAGAAGACTACCAGAAGC and reverse GTCATA-TAGCCGCCTCCACAG) and GAPDH (forward AGCAAGG AACTGAG-CAAGAGAGG and reverse GGGTCTGGGATGGAAATTGTGAGG).

### 2.15. Cleaning of the sample plates

The samples were incubated for 10 min in 20% TCA, for 30 min in RIPA buffer and for 30 min in 0.05% trypsin at 37 °C in a sonication bath, before being incubated in 70% of EtOH. Between the steps, the sample plates were washed with distilled water. Following this washing procedure, the sample plates were placed under UV light overnight.

## 2.16. *Galleria mellonella* infection model

*Staphylococcus capitis* was cultured as described before. The PMEDM silver-coated pins and non-modified control pins were inoculated 1:100 with *S. capitis* from the overnight culture (OD 1) in 1 ml TSB medium. After incubation at 37 °C for 24h, the samples were washed twice with PBS and then implanted into *Galleria mellonella* as described before [36]. Briefly, the infected pins were implanted at the second proximal segment on the ventral side of the larvae. The larvae were kept at room temperature for up to 6 days and the number of living larvae was counted every day.

## 2.17. Statistics

All data were presented as mean  $\pm$  SD. Data comparing two groups were analyzed by a *t*-test for statistical significance. Data with more than two groups were analyzed by a one-way ANOVA following a Dunnett's test as post-hoc test in case of a statistically significant ANOVA result. Data analyses were performed using GraphPad Prism version 6.00 for Windows (GraphPad Software, La Jolla California USA, [www.graphpad.com](http://www.graphpad.com)). Statistical significance was determined at level of  $P \leq 0.05$ .

## 3. Results

### 3.1. Characterization of silver modified surface layer

The distribution of silver embedded in the PMEDM modified surfaces using powder concentrations from 15 g/l to 20 g/l and discharge energies from 10  $\mu$ J to 125  $\mu$ J was analyzed. Fig. 2A shows representative

EDS analyses using nine different spectra spanning the total modified area. A quite uniform silver distribution ( $1.6 \pm 0.2$ ) % can be observed for all within the total modified area. Representative microscopic images of the cross-sectional cut through the modified layers are shown in Fig. 2B. The thickness of the modified layer generated using the low discharge energy of 10  $\mu$ J was about  $1.7^{+0.4}_{-0.2}$   $\mu$ m (thin layer). The use of 55  $\mu$ J resulted in a surface layer thicknesses of  $2.9^{+0.5}_{-0.6}$   $\mu$ m (medium layer) and 125  $\mu$ J of discharge energy resulted in  $4.1^{+1.3}_{-1.7}$   $\mu$ m (thick layer). Therefore, a thicker layer was generated when higher discharge energy was applied.

Top view SEM images of surfaces modified are shown in Fig. 2C. When applying higher discharge energy (from left to right), bigger craters were observed. Using backscattered electrons in the SEM analysis, silver is shown as bright color on the surface. Regarding microcracks, although applying relatively low discharge energy, they are visible on all surfaces.

Average silver contents of the samples with  $(10 \times 10)$  mm<sup>2</sup> and  $(3 \times 4)$  mm<sup>2</sup> modified area sizes are shown in Fig. 2D. For the samples with  $(10 \times 10)$  mm<sup>2</sup> modified area size, according to the limited maximum size of EDS spectra each with a size of approx.  $(4 \times 4)$  mm<sup>2</sup> were performed on each sample and the average silver content was calculated from these two spectra. It can be seen that with suitably adapting powder concentration and discharge energy, modified layers containing relatively similar silver content are possible whereby modified thicknesses can be varied.

Using confocal microscopy the surface roughness was analyzed. The average maximum profile height  $S_z$  shows higher values with increasing layer thickness and therefore increasing discharge energy. Representative surface topographic images are shown in Fig. 3a. The arithmetic

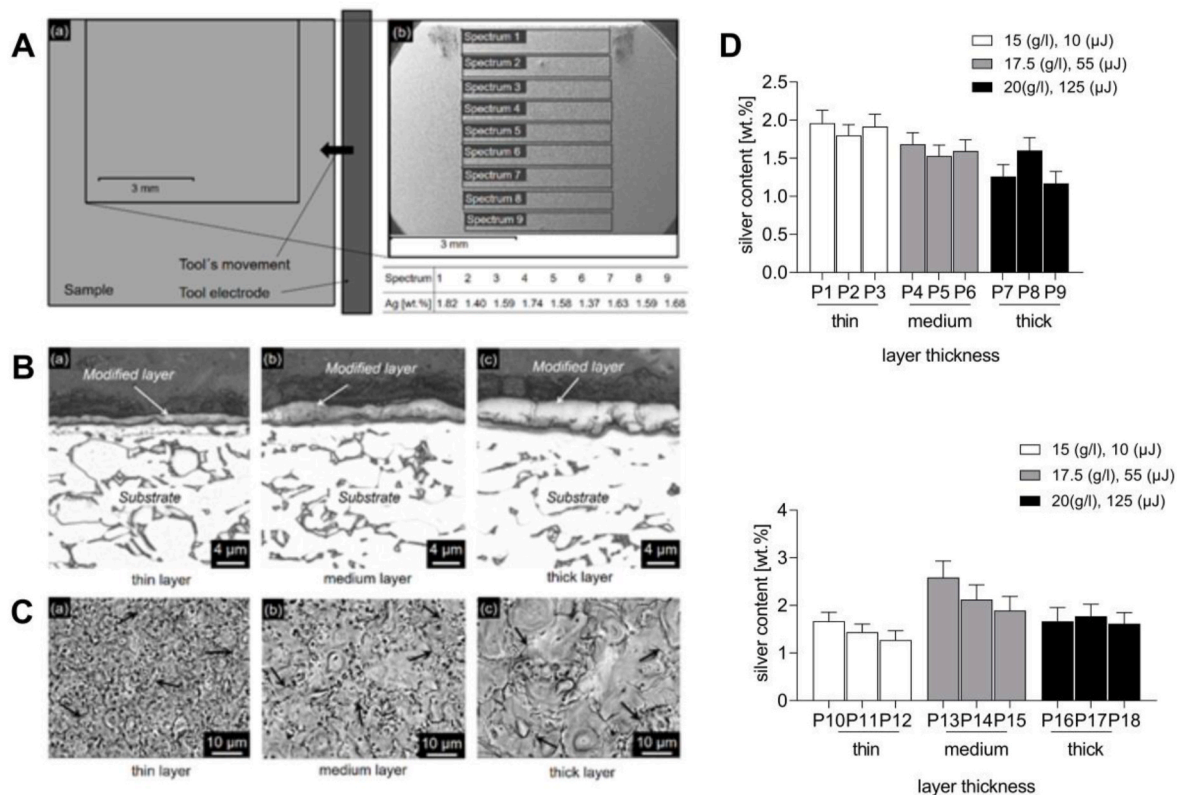


**Fig. 2.** (A) Distribution of deposited silver on the  $(10 \times 10)$  mm<sup>2</sup> modified area: (a) top view image of the sample surface; (b) analyzed silver contents of EDS spectra; sample modified using 17.5 g/l powder concentration and 55  $\mu$ J discharge energy. (B) SEM images showing the modified layers in cross-section after PMEDM using (a) 15 g/l, 10  $\mu$ J; (b) 17.5 g/l, 55  $\mu$ J and (c) 20 g/l and 125  $\mu$ J. (C) Top view SEM images of the modified surfaces using a backscattered electrons analysis: (a) 15 g/l, 10  $\mu$ J; (b) 17.5 g/l, 55  $\mu$ J and (c) 20 g/l and 125  $\mu$ J. Arrows point on microcracks. (D) Average silver contents (Mean  $\pm$  SD) of the investigated sample surfaces modified by applying different powder concentrations (g/l) and discharge energies ( $\mu$ J): upper panel: samples with  $(10 \times 10)$  mm<sup>2</sup> modified area size; Lower panel: samples with  $(3 \times 4)$  mm<sup>2</sup> modified area size.

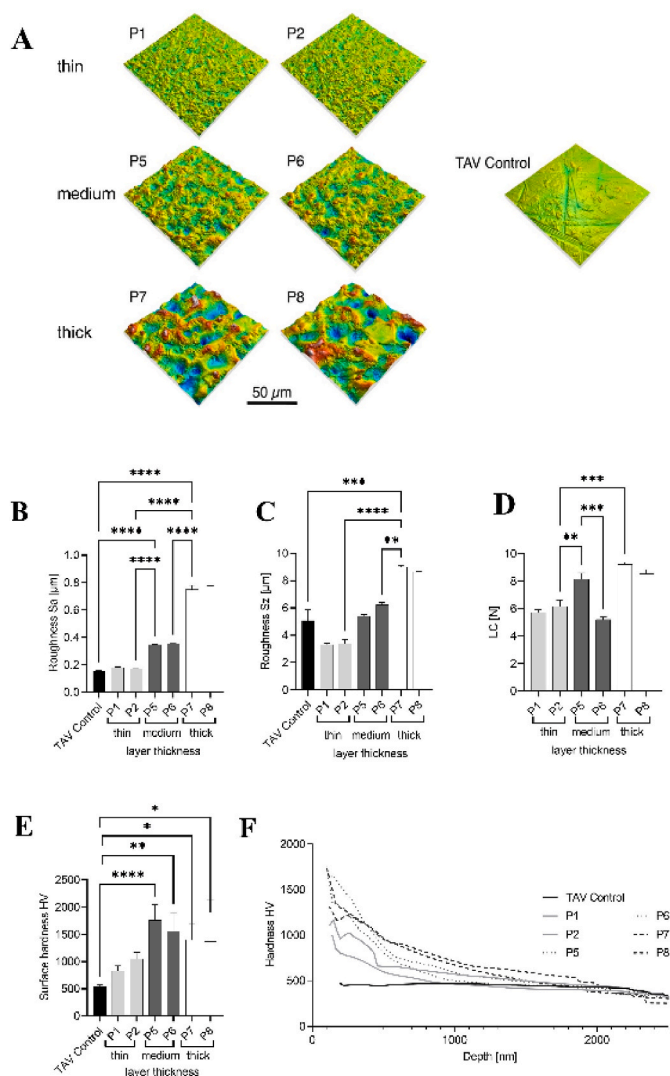


**Fig. 3.** (A) Representative 3D topographic images of the surfaces (B) measured arithmetic average roughness ( $S_a$ ) (C) average maximum profile height ( $S_z$ ) (D) LC values from layer adhesion scratch-test ( $n = 3 \pm \text{SD}$ ) scratch test (E) average indentation hardness constant load cycle ( $n = 6 \pm \text{SD}$ ) (F) dynamic measurements in sinus mode with depth profiles ( $n = 6$ ). The statistical analyses was performed using an ordinary one-way ANOVA with a Dunnett's post-hoc test. \* $p < 0.05$ , \*\* $p < 0.01$ , \*\*\* $p < 0.001$ , \*\*\*\* $p < 0.0001$ .

average roughness  $S_a$  of the thin layer showed the lowest roughness of  $S_a = 0.175 \pm 0.003 \mu\text{m}$ , which is similar to the unmodified TAV control. The thick layer shows the highest roughness of  $S_a = 0.75 \pm 0.05 \mu\text{m}$ , which is four times higher in comparison to the TAV control. The medium thick layers show a medium roughness of  $S_a = 0.35 \pm 0.004 \mu\text{m}$  (Fig. 3B). Similar results were observed for  $S_z$ , which showed higher values with increasing layer thickness and therefore discharge energy (thin:  $S_z = 0.35 \pm 0.18 \mu\text{m}$ ; medium:  $S_z = 0.57 \pm 0.17 \mu\text{m}$ ; thick:  $S_z = 0.87 \pm 0.1 \mu\text{m}$  (Fig. 3C).

Scratch tests were carried out to test the adhesion of the modified surface layer using a Rockwell diamond indenter. A tendency was observed that with increasing layer thickness the forces for layer failure were increased, which varied between  $5.69 \pm 0.43 \text{ N}$  for the thin layer P1 and  $9.24 \pm 0.23 \text{ N}$  for the thick layer P7 (Fig. 3D).

Nanoindentation tests ( $n = 6$ ) with constant load (Fig. 3E) and dynamic measurements in sinus mode (Fig. 3F) were used to analyze the hardness of the modified surface layers. All modified layers exhibit an increased hardness in the range of 830 HV (P1) - 1762 HV (P5) in comparison to the unmodified TAV control (500 HV). The medium thick

layers P5 and P6 show the highest surface hardness values, whereas the surface hardness of the thick layer (P7 and P8) was comparably high.

The dynamic measurements in sinus mode show that the hardness values of P7 and P8 declines less with a growing depth. At the depth range from 400 nm up to 2000 nm plates P7 and P8 exhibit the highest hardness values (Fig. 3F).

### 3.2. Reduced attachment of *Staphylococcus aureus* to silver modified surface layer independent of layer thickness

The quantification of *Staphylococcus aureus* (SH1000/pSB2035) adhesion to different silver modified surface layers is shown in Fig. 4. The *S. aureus* strain expresses a green fluorescent protein, therefore the green fluorescence on the surface represents attaching bacteria (Fig. 4A). The area of green fluorescence was measured for each image. An unmodified titanium aluminum vanadium (TAV) surface served as control sample. The samples were sorted according to the thickness of the silver modified surface layer in thin (light grey), medium (grey) and thick (white). The silver concentration for the tested samples was comparable (1.27%–2.59%) and is indicated in the upper left corner of the representative images (Fig. 4A). All silver-containing modified surfaces resulted in a significant reduction of adhering *S. aureus* compared to the control surface ( $p < 0.05$ ) (Fig. 4B). However, no difference was observed with regard to the layer thickness, as well as the minor changes in the silver concentration.

To exclude an influence of the differences in surface roughness of the silver modified surface layer on the number of adhering bacteria the amount of attaching bacteria was also tested against the average  $S_a$  values (Fig. 4C). Again, the amount of adhering bacteria on the different silver modified surface layers were compared to the control surface ( $S_a 0.150 \mu\text{m}$ ). All three silver layers showed a significant decrease in adhering *S. aureus* ( $p < 0.0001$ ) compared to the unmodified sample. As the  $S_a$  value for the unmodified control sample was comparable to the thin layer, no influence of the roughness on the number of adhering bacteria was observed.

In a next step, we analyzed the long-term antibacterial capacity of the silver modified surface layer. This time we used *S. capitis* for the adhesion to different silver modified surface layers for 7 days (Fig. 4D). The samples were again evaluated according to the thickness of the silver modified surface layer (thin: light grey, medium: grey and thick: white). Again, the area of green fluorescence was measured for each image. All silver-containing modified surfaces resulted in a reduction of adhering *S. capitis* compared to the control surface after 7 days of incubation (Fig. 4D). However, only the amount of bacteria detected on the medium and thick surface layer was significantly reduced in comparison to the unmodified TAV surface, that served as control sample (both  $p < 0.015$ ).

### 3.3. Silver does not inhibit the proliferation of attaching *S. aureus*

In order to test the influence of the surface silver content on the proliferation rate of adhering bacteria we performed an mKikumeGR proliferation assay. We used the *S. aureus* strain SH1000/pMD303 containing a plasmid that encodes a photo convertible green fluorescent protein (Fig. 5). The bacteria were incubated for 24 h on the sample plates and subsequently photo converted and then incubated again for 1h to measure the proliferation. During the photo conversion the green fluorescent protein is converted into a red fluorescent protein. During the proliferation a green fluorescent protein is produced, leading to a dilution of red fluorescence and an increase in green fluorescence in proliferating bacteria. Non-proliferating bacteria stay red fluorescent. Fig. 5A shows representative images of the mKikumeGR assay. The proliferation rate for each sample was normalized to the green fluorescence before photoconversion (100%) and a red fluorescence as marker for photoconversion efficacy (0%). We calculated the ratio between red and green fluorescence as parameter for the proliferation rate.

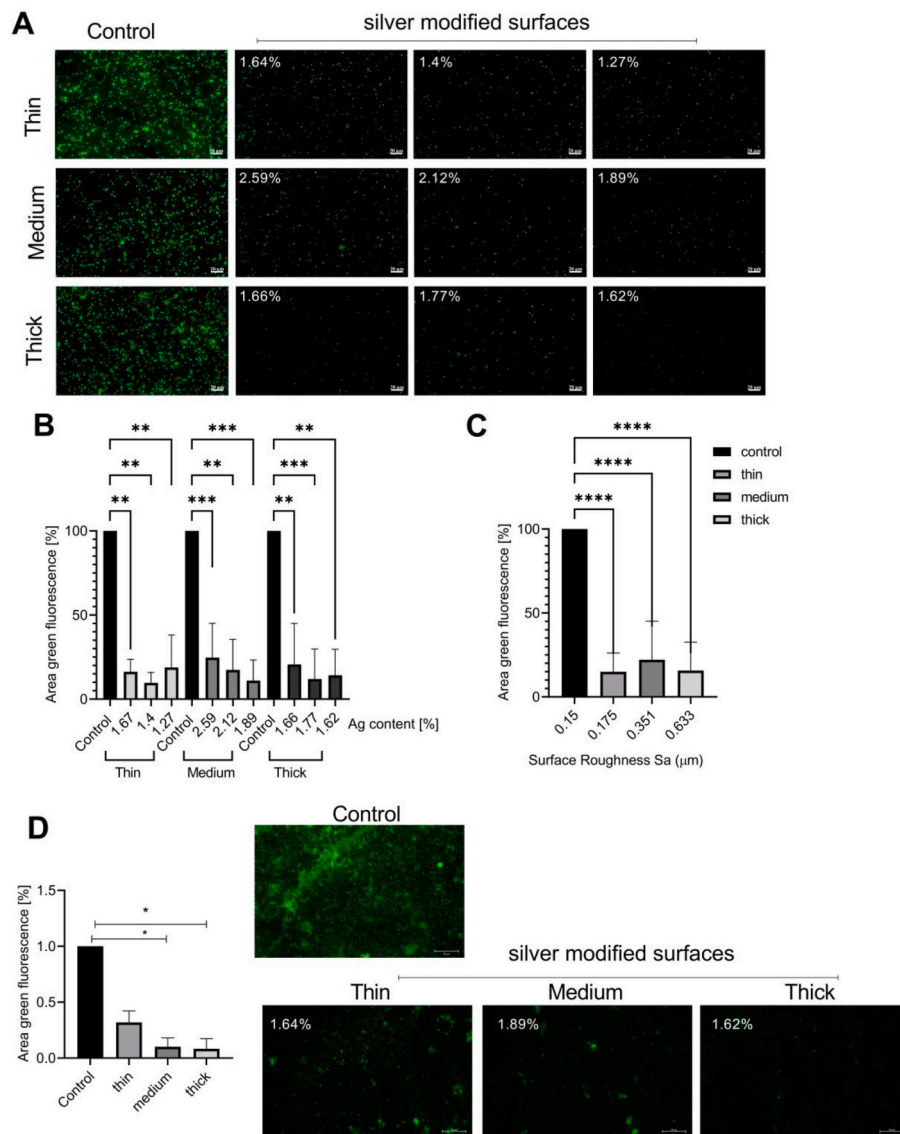


**Fig. 4. Significant reduction of *S. aureus* attachment to silver modified surface layer independent of layer thickness.** A) Representative images of the *S. aureus/pSB2035* were taken, every green dot represents one bacterium on the surface. The pictures were evaluated depending on the layer thickness and the surface roughness ( $\mu\text{m}$ ). The pictures were taken with a magnification of 630 fold (scale bar: 20  $\mu\text{m}$ ). (B) For the quantification of the fluorescent area the values are normalized to the unmodified TAV control for each experimental setup (Mean  $\pm$  SD). 5 images were taken per sample and the experiment was repeated in five independent setups (N = 5; n = 25). For the statistical evaluation a Kruskal Wallis test with Benjamini, Krieger and Yekutieli posthoc test was used (C) Quantification of fluorescent area representing *SH1000/pSB2035* attachment to silver modified surface layers evaluated depending on the surface roughness (Sa values). The values are normalized to the unmodified TAV control for each experimental setup (Mean  $\pm$  SD). 5 images were taken per sample and the experiment was repeated in five independent setups (N = 5; n = 25). D.) Representative images of the *S. capitis* were taken, every green dot represents one bacterium on the surface. The pictures were evaluated depending on the layer thickness and the surface roughness ( $\mu\text{m}$ ). The pictures were taken with a magnification of 630 fold (scale bar: 50  $\mu\text{m}$ ). For the quantification of the fluorescent area, the values are normalized to the unmodified TAV control for each experimental setup (Mean  $\pm$  SD). 5 images were taken per sample and the experiment was repeated in five independent setups (N = 3; n = 15). For the statistical evaluation a Friedman test with Benjamini, Krieger and Yekutieli posthoc test was used; \*p < 0.05, \*\*p < 0.01, \*\*\*p < 0.001, \*\*\*\*p < 0.0001.

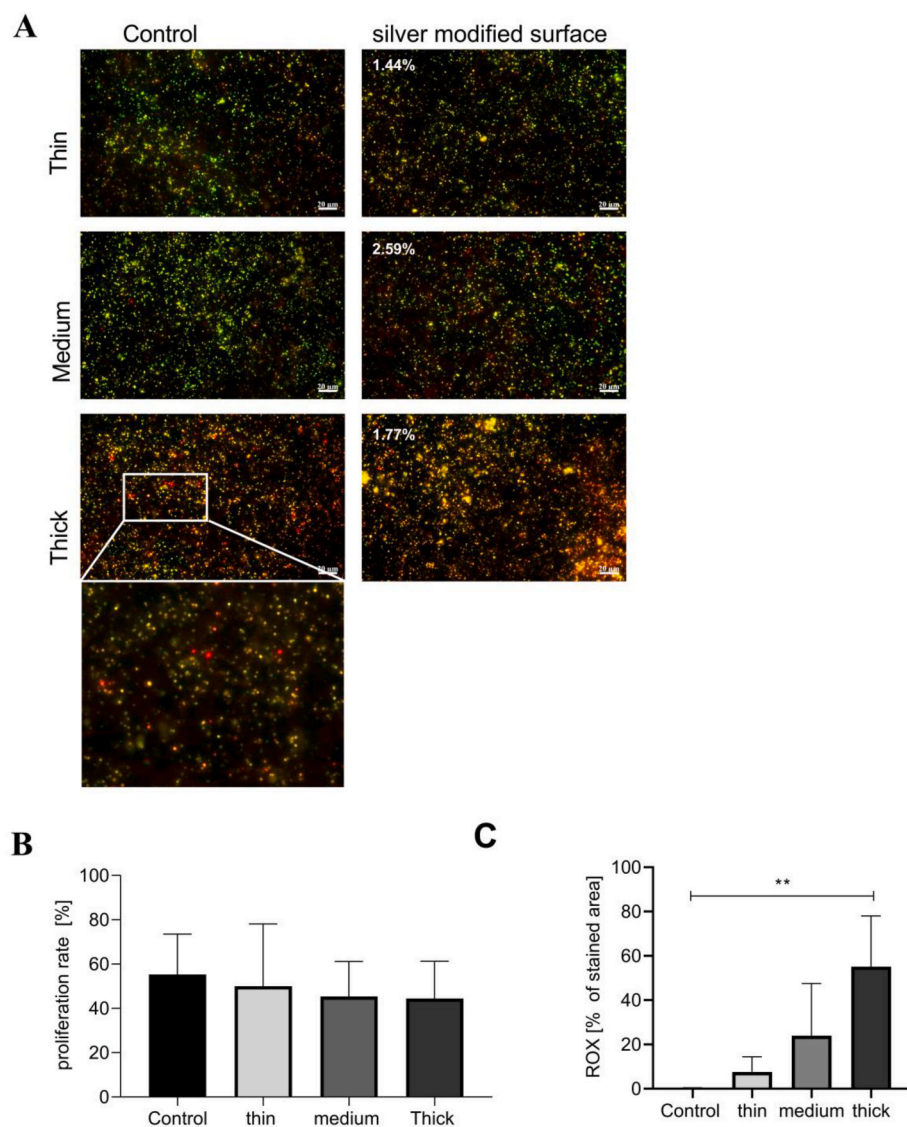
Therefore, higher values correlate with higher proliferation rates and low values with low proliferation rates. Fig. 5B shows the comparison of the proliferation ratios for the tested samples. No significant difference between the silver modified surfaces and the control surface was observed with regard to the proliferation rate of *S. aureus* (Mean  $\pm$  SD; control:  $55.30 \pm 5.26$  thin:  $50.07 \pm 8.47$ , medium:  $43.37 \pm 5.00$ , thick:  $44.45 \pm 5.09$ ). When we investigated the oxidative stress induced by the silver integration into the surface we observed significantly more ROX positive bacteria on thick silver modified surfaces compared to the control ( $p = 0.0003$ ) (Fig. 5C). We observed a trend of increasing ROX staining with increasing thickness of the silver modified layer, which did only reach statistical significance for the thick layer.

### 3.4. Reduced osteoclast formation, but no influence of silver modified surface layers on *in vitro* ossification

Since osteoclasts play an essential role in endoprosthesis integration and bone restructuring processes, bone marrow macrophages (BMMs) were differentiated by the addition of RANKL and M-CSF for 12 days to osteoclasts on the silver modified samples with the TAV control sample. We stained the osteoclasts with Phalloidin (red) to visualize the cytoskeleton and DAPI (blue) for cell nuclei. Osteoclasts were defined to

have more than five nuclei. Fig. 6A indicates the average numbers of osteoclasts on the different silver modified surface layers and the control sample. No osteoclast formation was observed on any silver modified surface, whereas on the control samples an average of  $6.3 \pm 0.33$  osteoclasts was counted (N = 3). The representative images show on the control (TAV) large osteoclasts on the surface with the typical formation of multinucleated cells (blue) that are clearly surrounded by the cytoskeleton (red). On the right a representative picture of the silver surface modified sample without multinuclear cells being present is shown (Fig. 6A). To verify the observation that less or no osteoclasts are formed on the silver-modified surfaces, we performed a quantitative real-time PCR for osteoclast marker genes. We observed a significant reduced expression of tartrate-resistant acid phosphatase (TRAP) on silver modified platelets compared to the control surface ( $p = 0.003$ ), as well as cathepsin K ( $p = 0.0004$ ) (Fig. 6B and C).

To test the bone forming activity of osteoblasts on the silver coatings, human SaOs2 cells were incubated for 24 h on the different silver modified samples and the metabolic activity was analyzed using the WST assay. This assay gives a first indication about cytotoxic effects of the silver in the modified surface. No changes in the metabolic activity were observed, as indicated by changes in the WST assay depending on the silver modified surface (Fig. 6C). Furthermore, to exclude cytotoxic



effects, a TUNEL assay was performed to investigate cell death induced by the silver modified surfaces. No significant increase in TUNEL positive cells were detected after incubation of SaOs-2 cells for 24 h on the different surfaces (Suppl Fig. 1). As silver has been shown to induce oxidative stress in cells, DHE assays were performed to evaluate the formation of reactive oxygen species (ROS) in SaOs-2 cells depending on the cultivation on the different silver modified surfaces. No significant effect on the ROS formation, as measured by DHE, was observed (Fig. 6D). Representative images of the positive and negative control, as well as the DHE staining of SaOs-2 cells on the different surfaces are given in the bottom panel. To investigate the bone forming activity of SaOs-2 osteoblast like cells, these cells were differentiated for 10 days under ossifying conditions on the different platelets. To quantify the amount of *in vitro* bone formation an alizarin Red assay was performed as shown on the left-handed diagram (Fig. 6E). Again, the samples were analyzed according to the thickness of the silver modified surface layer (normalized to TAV control). No significant effect of the silver modified surface layers on the osteoblasts mediated *in vitro* mineralization, as measured by the alizarin red assay, was observed.

**Fig. 5. Silver does not inhibit the proliferation of attaching *S. aureus*** (A) Representative images of *SH1000/pMD303* on control or silver modified surfaces. Every red dot represents a photo converted bacterium and every green dot shows a proliferating bacterium. The pictures were evaluated according to the layer thickness. The pictures were taken with a magnification of 630 fold (scale bar: 20  $\mu$ m). (B) For the quantification, we analyzed the proliferation rate of *SH1000/pMD303* on different silver modified based on the layer thickness compared to unmodified TAV controls (Mean  $\pm$  SD). 5 images were taken per sample and the experiment was repeated in five independent setups (N = 5; n = 25). The statistical evaluation was performed using a One-way ANOVA with Dunnett's posthoc test. (C) ROX assay for quantification of oxidative stress in adhering bacteria. For the quantification, we analyzed the ROX stained area on different silver modified based on the layer thickness compared to TAV controls (Mean  $\pm$  SD). 5 images were taken per sample and the experiment was repeated in five independent setups (N = 5; n = 25). The statistical evaluation was performed using a One-way ANOVA with Dunnett's posthoc test (F (3, 16) = 10.53; p = 0.0005). \*p < 0.05, \*\*p < 0.01, \*\*\*p < 0.001, \*\*\*\*p < 0.0001.

### 3.5. Silver modified surfaces exhibit a marked *in vivo* antibacterial capacity

As a final proof of the antibacterial property of the investigated silver modified TAV surface, we performed an *in vivo* infected implant model using larvae of *Galleria mellonella*. These insect larvae were used as a model for implant associated *S. capitis* infections and to test *in vivo* biocompatibility. In preliminary experiments, we have shown that the larvae with 4–5 mm TAV pins that had a diameter of 0.8 mm were as active and viable as the non-implanted controls. The implantation of TAV pins did not cause adverse effects, such as metal toxicity, restricted mobility, negative impact on wound healing or melanisation at the site of implantation (Fig. 7 A). To investigate the potential antibacterial effect, the silver modified and unmodified TAV pins were incubated with *S. capitis* and implanted in the larvae. We used unmodified TAV pins without prior incubation with bacteria as negative control. Our data clearly show that the survival of larvae was significantly increased with the silver modified implants compared to the implants without silver in the surface layer (F (2, 14) = 9.840; p = 0.0021). Without silver modification, most larvae were dead after 3 days, whereas about 60% of larvae with silver implants survived at this time. The experiment was aborted after 6 days. At this time point still about 25% of larvae with silver implants survived.

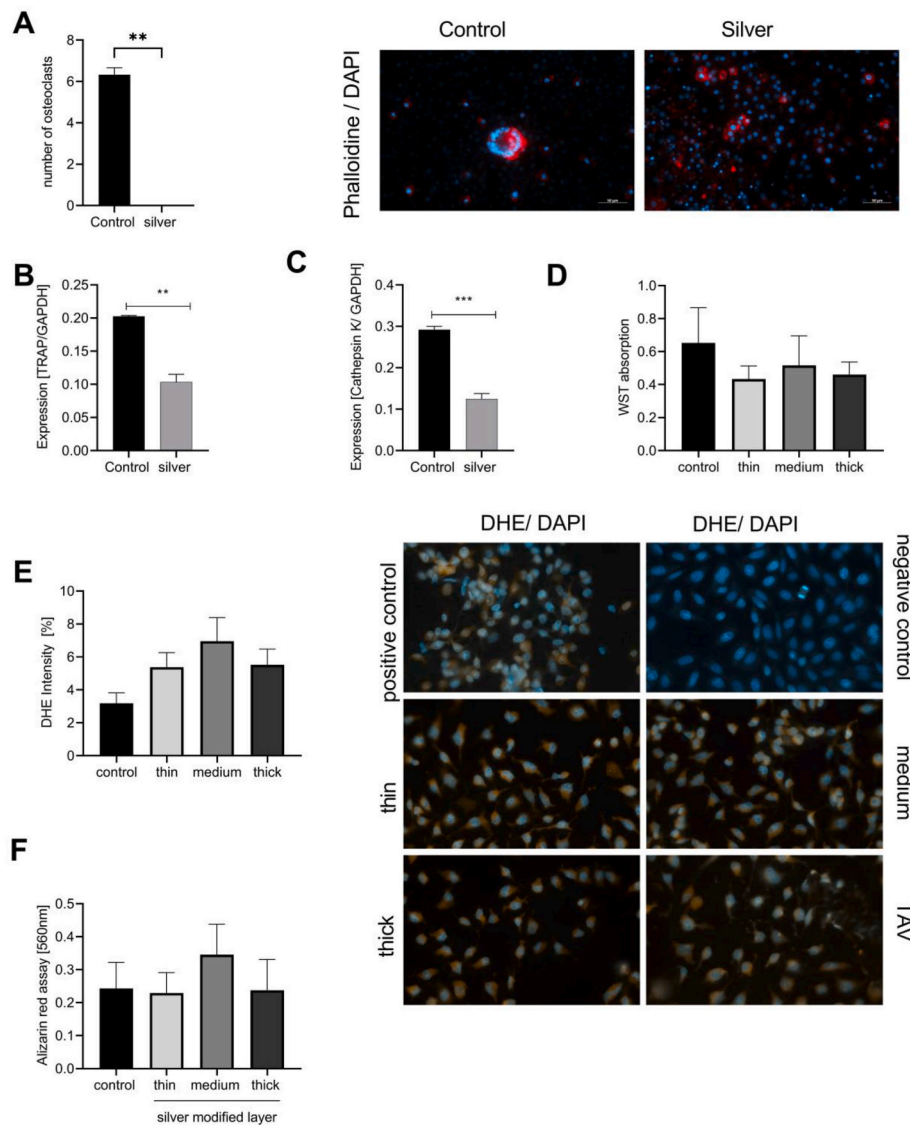


**Fig. 6. Reduced osteoclast formation, but no influence of silver modified surface layers on *in vitro* ossification.** (A) The graph shows the statistical difference between the number of osteoclasts on a TAV control and the silver-containing samples; silver-containing samples are summarized under silver;  $N = 3$ ; values are given with Mean  $\pm$  SD, the statistical evaluation was performed using the Welch's *t*-test;  $**p = 0.028$ . Representative images of osteoclasts from BMMs on TAV controls. The cells were stained with Phalloidin (red) to visualize the cytoskeleton and DAPI (blue) for the cell nuclei; a magnification 400x (scale bar: 50  $\mu$ m) was used. (B.) Quantitative RT-PCR of TRAP expression in wt murine osteoclasts after 11 days of differentiation on silver-modified surfaces or the unmodified TAV control. GAPDH was used as housekeeping gene. The values are normalized to the control and analyzed using an unpaired *t*-test for statistical significance. (C) Quantitative RT-PCR of cathepsin K expression in wt murine osteoclasts after 11 days of differentiation on silver-modified surfaces or the unmodified TAV control. GAPDH was used as housekeeping gene. The values are normalized to the control and analyzed using an unpaired *t*-test for statistical significance. (D.) WST Assay for metabolic activity of SaOs-2 cell on the different silver modified samples. The experiment was repeated in five independent setups ( $N = 5$ ). No difference in the metabolic activity was observed. The statistical evaluation was performed using a One-way ANOVA with Dunnett's posthoc test ( $F(3, 19) = 0.42$ ;  $p = 0.74$ ). (E.) The intensity of DHE staining was evaluated for each silver condition. 5 images were taken per sample and the experiment was repeated in five independent setups ( $N = 5$ ;  $n = 25$ ). The statistical evaluation was performed using a One-way ANOVA with Dunnett's posthoc test ( $F(3, 16) = 3.078$ ,  $p = 0.058$ ). Representative images are shown for the positive control as well as the negative control (DAPI: blue, DHE: red). (F) Alizarin Red Ossification Assay of SaOs 2 cells was performed to calculate the calcification. No significant differences between the TAV control and the silver coatings were analyzed on different silver modified surfaces clustered based on the layer thickness and silver content compared to unmodified TAV controls (one-way ANOVA: with Dunnett's post-hoc was performed;  $ns > 0.05$ ).  $*p < 0.05$ ,  $**p < 0.01$ ,  $***p < 0.001$ ,  $****p < 0.0001$ .

To verify the silver content in the manufactured implant pins, we analyzed the surface silver concentration using SEM-EDS. All samples contained more than 1.5% of silver, whereas only 0.45% of silver was detected in the samples without silver flushing (negative control) (Fig. 7B).

#### 4. Discussion

PJIs are one of the most common reasons for revisions surgeries [1]. To reduce the incidence of PJIs, it has been suggested to coat endoprosthesis materials with antibacterial substances, e.g. antibiotics or metals with antibacterial properties such as silver [37,38]. The antibacterial effect of silver has been investigated *in vitro* as well as *in vivo* in animal studies [24,39,40]. We have shown previously that even at low silver concentrations the amount of *S. aureus* attaching to the PMEDM silver modified surfaces was reduced *in vitro* [24]. However, whether the thickness of the silver layer produced by PMEDM affected the attachment of bacteria to the surface and whether the proliferation rate of the bacteria would also be reduced by silver was not investigated so far.

Independent of the antibacterial effect of the modified implant

surface, the biocompatibility, as well as surface characteristics and mechanical properties need to be considered [41]. It has been reported that  $Ag^+$  exhibited a cytotoxic effect in eukaryotic cells, especially osteoblast like cells [42–44]. A cytotoxic effect of these nanoparticles might be due to an initial  $Ag$  burst [45]. However, when applying PMEDM to integrate silver in the surface layer of the implant material no loose nanoparticles remain on the sample surface, but the silver incorporated into the surface layer of the implant serves for antibacterial effects [24].

Our data indicate that, in comparison to the surface modified using cylindrical tool electrode that the utilization of sheet tool electrodes has significantly enhanced the uniformity of deposited silver distribution on the modified surface. The use of the cylindrical tool electrode in our previous study resulted in a silver distribution within the range of  $6.6 \pm 2.5\%$  silver content has been reported when using powder concentration of 15 g/l and discharge energy of 10  $\mu$ J [24]. In this study a range of  $1.8 \pm 0.2\%$  silver content was obtained using a sheet tool electrode with the same machining parameters, which indicates a more uniform silver concentration throughout the modified surface.

The results of the surface characterization showed an increase in

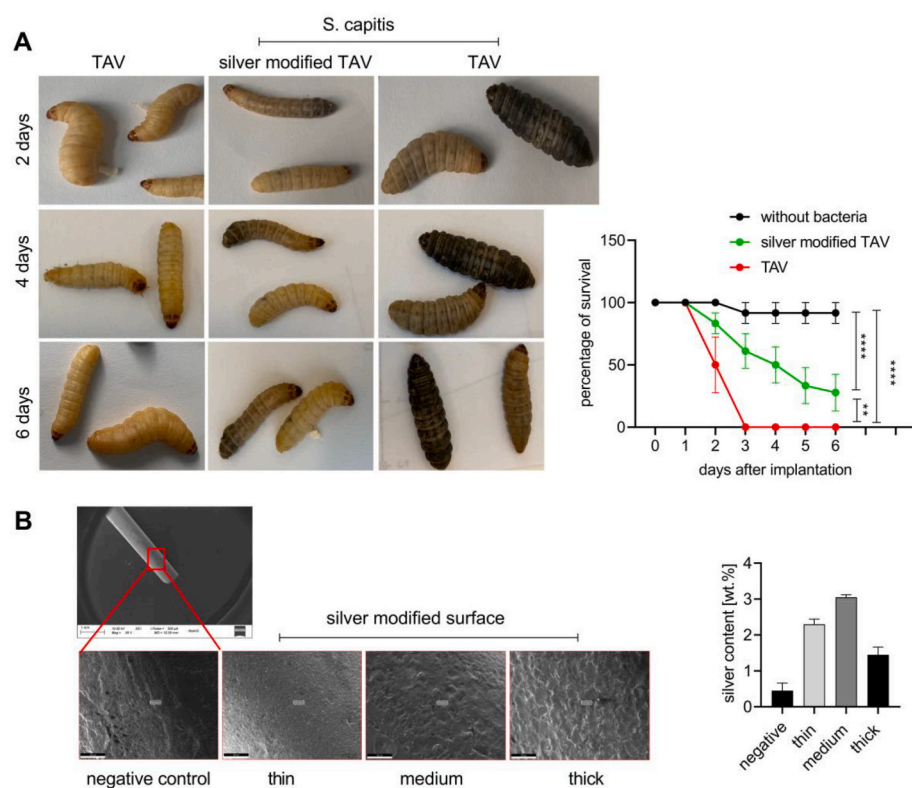


**Fig. 7. Silver modified surfaces exhibit a marked *in vivo* antibacterial capacity** (A) Representative images of *Galleria mellonella* larvae at the respective time points during the *in vivo* implant infection model (day 2, 4 and 6). The dark brown larvae are dead, whereas the light brown larvae are alive. A beginning darkening of larvae (melanisation) at the implantation site shows the spreading of infection and induction of immune response. For the quantification, we analyzed the number of living larvae each day in three independent experiments (Mean  $\pm$  SD). (N = 3; n = 6–12). The statistical evaluation was performed using a two-way ANOVA with Tukey posthoc test. (B) SEM images showing the implant pin (top left). The red square indicates the area for SEM EDX analyses of the modified layers in a top view. The average silver contents (Mean  $\pm$  SD) of the investigated sample surfaces are given in the graph.  $p = 0.0005$ . \* $p < 0.05$ , \*\* $p < 0.01$ , \*\*\* $p < 0.001$ , \*\*\*\* $p < 0.0001$ .

surface roughness for the medium and especially for the thick modified surface layers. This increase is due to the higher discharge energy, inducing bigger and deeper craters, as well as larger amount of the molten and re-solidified material, leading to a rougher surface. However, the results for the layer hardness do not reflect this linear behavior. The hardness of all modified layers was significantly increased as compared to the substrate control value. The highest hardness was achieved at 55  $\mu$ J of discharge energy which resulted in a medium layer thickness. The layer thickness showed no systematic change due to the high standard deviations.

The adhesion of modified layers on the substrate was investigated by scratch tests. Neither the thin, medium nor the thick layers showed an adhesion failure. However, the thickness of modified layers affects the force of scratches significantly, whereby the force tends to increase for thicker modified layers.

In order to study the influence of the silver modified surface layer thickness and its roughness on the antimicrobial capacity, three different layer thickness with similar silver contents were produced. The thin layer had a thickness of  $1.7^{+0.4}_{-0.2}$   $\mu$ m, the medium layer of  $2.9^{+0.5}_{-0.6}$   $\mu$ m and the thick layer of  $4.1^{+1.3}_{-1.7}$   $\mu$ m. The silver concentration within these layer was about 1.27%–1.77%. This range of silver concentration was chosen based on the previously published study showing a low attachment of *S. aureus* at this silver concentration and no further reduction of attaching *S. aureus* with higher silver concentrations [24]. The attachment of *S. aureus* was analyzed after 24h of incubation, reflecting a short term exhibition. At this time the bacteria would reach the stationary growth phase, where they stop growing but are still metabolically active [46]. As expected, all three thicknesses of surface layers resulted in a significant reduction ( $p < 0.0001$ ) of adhering bacteria (Fig. 4). This observation is in line with a previous publication showing the inhibition of *Staphylococcus* spp. growth by silver [47,48].

The influence of the surface roughness on the adhesion of bacteria has already been proven in a number of other studies, as the surface roughness has been shown to be a critical determinant of bacterial attachment to implant surfaces [49,50]. We did not observe an influence

of minor surface roughness changes on the attachment of bacteria in our experiments (Fig. 4B). The thin silver surfaces had an average  $R_a$  of 0.175  $\mu$ m, which was slightly increased in the medium group ( $R_a$ : 0.351  $\mu$ m) and the highest  $R_a$  value was measured on the thick layer with  $R_a$  of 0.633  $\mu$ m. No correlation of the surface roughness with the amount of adhering *S. aureus* was observed. This might be due to the fact that the roughness of our samples varies between  $R_a$ : 0.1–0.6  $\mu$ m which is below the size of a bacterium (approx. 1  $\mu$ m). Surfaces with higher roughness have been proposed to be very attractive for adhering bacteria [51]. Interestingly, the silver integrated in the surface layer could abolish the effect of the increased roughness.

However, silver has also been described to inhibit bacterial cell division and thereby proliferation [31]. To investigate the proliferation inhibiting effect of our silver modified surface we used the *S. aureus* mKikume strain (Fig. 5). This *S. aureus* strain expresses the photo convertible proliferation reporter mKikumeGR [52]. Our data showed that there was no significant influence of the silver modified surface on the proliferation rate of attaching *S. aureus*. This indicates that the silver content of the surface has no effect on the division of bacteria, and only inhibits their adhesion. A previous study described that silver ions were mostly released after the first hours of implantation [18]. However, the authors used a different silver modification setup, where silver ions were included in silica-based bioactive glass. As the silver ions in our study are alloyed in the surface material, no significant loss of silver ions over time is expected. It has been suggested that silver might inhibit the adhesion of bacteria by producing nanocurrents between precious and base metals within the alloy [53]. Due to the integration of silver in the titanium surfaces the proposed nanocurrents could have a long-term effect on the adhesion of bacteria. Our data confirm a long-term effect of our silver modified surface over seven days of culturing on the *Staphylococcus* adhesion, indicating that the silver ions alloyed in the surface layer have a long-term antibacterial effect (Fig. 4D).

Silver has been described to have a cytotoxic effects which can lead to cell death of osteoblasts [54]. In contrast, other studies observed that a low concentration of silver had a positive effect on osteogenic

maturation [55]. To test the effect of the PMEDM modified silver surfaces on the bone forming capacity of osteoblasts we used the SaOs2-cell line. SaOs-2 as well as MG-63 are frequently used osteosarcoma cell lines as model systems for investigating osteogenic cell behavior on different biomaterials. These cell lines have the capacity to undergo osteoblastic differentiation in response to osteogenic medium incubation without the variability of human or primary cells [56]. SaOs2 cells are an established model for ossification assays on implant materials [57]. SaOs2 cells were grown for 10 days on silver surfaces under ossifying culture conditions, as a control a Ti–6Al–4V surface was used. The bone forming capacity was analyzed using the Alizarin-Red-Assay. No significant difference was found between the control and silver surfaces (Fig. 6). Overall, it was shown that silver had no negative effect on the bone formation. Suggesting, that the silver surfaces having a similar biocompatibility with regard to the calcification compared to the control surface. This is in line with previous studies, that even described a positive effect on cell spreading using the osteoblastic cell lines MG63 and MC3T3 [58,59]. However, osteoblasts also showed increased cell stress after incubation with silver nanoparticles stabilized in a matrix for 21 days [48]. No increase in osteoblastic cell stress was observed on the silver integrated surface layers of this study. Neither the WST assay for metabolic activity, nor the TUNEL-assay for cell death and additionally the DHE assay for oxidative stress showed a significant difference between the control and the silver modified surfaces using SaOs2 cells. We think that the reason for this observation is the low amount of silver ion release from the surface layer due to the fact that the silver is alloyed into the TAV alloy during the PMEDM process. Furthermore, there are studies indicating that bacteria are more sensitive towards silver compared to eukaryotic cells [60,61]. This fact could explain the induction of oxidative stress in bacteria, whereas no such effect was observed in osteoblast-like cells.

The interaction of osteoblasts and osteoclasts is important for the process of bone remodeling. However, an increased formation of osteoclasts would result in increased bone resorption and bone loss around the implant [51]. Silver nanoparticles have been previously described to the inhibition of osteoclast formation [62,63]. Therefore, we wanted to investigate how the silver modified surfaces impact on the osteoclast differentiation. In contrast to the titanium surface, no osteoclasts formed on the silver modified surfaces (Fig. 6A). This observation was corroborated by the fact that less osteoclastic marker genes were expressed by the cells on the silver modified surface compared to the TAV surface (Fig. 6B and C). This finding indicates that there would be no induction of osteoclast formation, but equal amounts of osteoblast function, that might result in a better osseointegration of the silver modified implant materials.

In a final experiment, we investigated the *in vivo* antibacterial capacity of the silver modified surface using *S. capitis* incubated TAV pins in the *Galleria mellonella* implant model [36,64]. Our experiments show that the survival of *Galleria mellonella* larvae was significantly increased with infected silver modified surface pins compared to infected TAV pins. These data indicate that indeed the PMEDM silver surface modification can reduce periprosthetic infections (Fig. 7).

## 5. Conclusion

We show that already small amounts of silver exhibit a significant antibacterial capacity, while at the same time the osseointegrative function of osteoblasts on the modified surface is not negatively influenced. There might even be a positive effect due to the reduced amount of osteoclasts formed on the silver modified surface. Therefore, PMEDM using silver nano-powder admixed to the dielectric represents a promising technology to shape and concurrently modify implant surfaces to reduce infections while at the same time optimizing bone ingrowth of endoprosthesis.

## Ethics approval and consent to participate

Not applicable, as there we have used no human samples and no animal experiments were performed.

## CRediT authorship contribution statement

**Hilmar Büsselmeier:** Investigation, Methodology, Writing – original draft. **Ann-Kathrin Meinshausen:** Investigation, Methodology, Writing – original draft. **Viet Duc Bui:** Investigation, Methodology. **Joachim Döring:** Investigation, Validation. **Vadym Voropai:** Investigation, Methodology. **Adrian Buchholz:** Methodology, Investigation. **Andreas J. Mueller:** Methodology. **Karsten Harnisch:** Investigation, Methodology, Validation. **André Martin:** Supervision, Validation, Conceptualization. **Thomas Berger:** Investigation, Methodology. **Andreas Schubert:** Supervision, Conceptualization, Funding acquisition, Writing – review & editing. **Jessica Bertrand:** Investigation, Methodology, Supervision, Conceptualization, Funding acquisition, Writing – review & editing.

## Declaration of competing interest

The authors have no financial or personal interest or belief that could affect their objectivity with regard to the present manuscript.

## Acknowledgements

Funding was provided by the DFG BE 4328/12-1 and SCHU 1484/33-1.

## Appendix A. Supplementary data

Supplementary data to this article can be found online at <https://doi.org/10.1016/j.bioactmat.2023.08.019>.

## References

- [1] N.G. Wetters, T.G. Murray, M. Moric, S.M. Sporer, W.G. Paprosky, C.J. Della Valle, Risk factors for dislocation after revision total hip arthroplasty, *Clin. Orthop. Relat. Res.* 471 (2) (2013) 410–416.
- [2] A.TaW. Zimmerli, Diagnosis and treatment of implant-associated septic arthritis and osteomyelitis, *Curr. Infect. Dis. Rep.* 10 (2008) 394–403.
- [3] T.K.O.S. Fehring, T.F. Caltin, J.B. Mason, Articulating versus static spacers in revision total knee arthroplasty for sepsis, *Orthopaed. Relat. Res.* 380 (2000) 9–16.
- [4] Alfred L. Goldberg, I.C. K, Koji Furuno, Julie M. Fagan, Vickie Baracos, Activation of protein breakdown and prostaglandin E2 production in rat skeletal muscle in fever is signaled by a macrophage product distinct from interleukin 1 or other known monokines, *J. Clin. Invest.* 81 (1988) 1378–1383.
- [5] M. Smucny, M.E. Menendez, D. Ring, B.T. Feeley, A.L. Zhang, Inpatient surgical site infection after shoulder arthroplasty, *J. Shoulder Elbow Surg.* 24 (5) (2015) 747–753.
- [6] S.M. Kurtz, K.L. Ong, E. Lau, K.J. Bozic, D. Berry, J. Parvizi, Prosthetic joint infection risk after TKA in the Medicare population, *Clin. Orthop. Relat. Res.* 468 (1) (2010) 52–56.
- [7] A.J. Tande, R. Patel, Prosthetic joint infection, *Clin. Microbiol. Rev.* 27 (2) (2014) 302–345.
- [8] D.R. Murdoch, S.A. Roberts, V.G. Fowler Jr., M.A. Shah, S.L. Taylor, A.J. Morris, G. R. Corey, Infection of orthopedic prostheses after *Staphylococcus aureus* bacteremia, *Clin. Infect. Dis.* 32 (4) (2001) 647–649.
- [9] W.F. Oliveira, P.M.S. Silva, R.C.S. Silva, G.M.M. Silva, G. Machado, L. Coelho, M.T. S. Correia, *Staphylococcus aureus* and *Staphylococcus epidermidis* infections on implants, *J. Hosp. Infect.* 98 (2) (2018) 111–117.
- [10] J.R. Lentino, Prosthetic joint infections: bane of orthopedists, challenge for infectious disease specialists, *Clin. Infect. Dis.* 36 (9) (2003) 1157–1161.
- [11] M. Cloutier, D. Mantovani, F. Rosei, Antibacterial coatings: challenges, perspectives, and opportunities, *Trends Biotechnol.* 33 (11) (2015) 637–652.
- [12] C.P. Guo, F. Cheng, G.L. Liang, S. Zhang, Q.J. Jia, L.H. He, S.X. Duan, Y.K. Fu, Z. H. Zhang, M. Du, Copper-based polymer-metal-organic framework embedded with Ag nanoparticles: long-acting and intelligent antibacterial activity and accelerated wound healing, *Chem. Eng. J.* (2022) 435.
- [13] B. Benli, C. Yalm, The influence of silver and copper ions on the antibacterial activity and local electrical properties of single sepiolite fiber: a conductive atomic force microscopy (C-AFM) study, *Appl. Clay Sci.* 146 (2017) 449–456.
- [14] M. Chen, Q. Yu, H. Sun, Novel strategies for the prevention and treatment of biofilm related infections, *Int. J. Mol. Sci.* 14 (9) (2013) 18488–18501.

- [15] M. Mohiti-Asli, B. Pourdeyhi, E.G. Lobo, Novel, silver-ion-releasing nanofibrous scaffolds exhibit excellent antibacterial efficacy without the use of silver nanoparticles, *Acta Biomater.* 10 (5) (2014) 2096–2104.
- [16] Z.Y. Sun, C.X. Fan, X.P. Tang, J.H. Zhao, Y.H. Song, Z.B. Shao, L. Xu, Characterization and antibacterial properties of porous fibers containing silver ions, *Appl. Surf. Sci.* 387 (2016) 828–838.
- [17] H. Wafa, R.J. Grimer, K. Reddy, L. Jeys, A. Abudu, S.R. Carter, R.M. Tillman, Retrospective evaluation of the incidence of early periprosthetic infection with silver-treated endoprostheses in high-risk patients: case-control study, *Bone Joint Lett.* J 97-B (2) (2015) 252–257.
- [18] A. Cochis, J. Barberi, S. Ferraris, M. Miola, L. Rimondini, E. Verne, S. Yamaguchi, S. Spriano, Competitive surface colonization of antibacterial and bioactive materials doped with strontium and/or silver ions, *Nanomaterials* 10 (1) (2020).
- [19] B. Khalandi, N. Asadi, M. Milani, S. Davaran, A.J.N. Abadi, E. Abasi, A. Akbarzadeh, A review on potential role of silver nanoparticles and possible mechanisms of their actions on bacteria, *Drug Res.* 11 (2017) 70–76, 02.
- [20] Y. Qing, L. Cheng, R. Li, G. Liu, Y. Zhang, X. Tang, J. Wang, H. Liu, Y. Qin, Potential antibacterial mechanism of silver nanoparticles and the optimization of orthopedic implants by advanced modification technologies, *Int. J. Nanomed.* 13 (2018) 3311–3327.
- [21] R. Zhang, P. Lee, V.C. Lui, Y. Chen, X. Liu, C.N. Lok, M. To, K.W. Yeung, K.K. Wong, Silver nanoparticles promote osteogenesis of mesenchymal stem cells and improve bone fracture healing in osteogenesis mechanism mouse model, *Nanomedicine* 11 (8) (2015) 1949–1959.
- [22] Y. Deng, X.Y. Shi, Y. Chen, W.Z. Yang, Y. Ma, X.L. Shi, P.G. Song, M.S. Dargusch, Z. G. Chen, Bacteria-triggered pH-responsive osteopotentiating coating on 3D-printed polyetheretherketone scaffolds for infective bone defect repair, *Ind. Eng. Chem.* 59 (26) (2020) 12123–12135.
- [23] S. Jain, V. Parashar, Critical review on the impact of EDM process on biomedical materials, *Mater. Manuf. Process.* 36 (15) (2021) 1701–1724.
- [24] V.D. Bui, J.W. Mwangi, A.-K. Meinshausen, A.J. Mueller, J. Bertrand, A. Schubert, Antibacterial coating of Ti-6Al-4V surfaces using silver nano-powder mixed electrical discharge machining, *Surf. Coating. Technol.* 383 (2020), 125254.
- [25] A. Kedziora, M. Speruda, E. Krzyzewska, J. Rybka, A. Lukowiak, G. Bugla-Ploskonska, Similarities and differences between silver ions and silver in nanofoms as antibacterial agents, *Int. J. Mol. Sci.* 19 (2) (2018).
- [26] S. Sutterlin, E. Tano, A. Bergsten, A.B. Tallberg, A. Melhus, Effects of silver-based wound dressings on the bacterial flora in chronic leg ulcers and its susceptibility in vitro to silver, *Acta Derm. Venereol.* 92 (1) (2012) 34–39.
- [27] L. Rizzello, P.P. Pompa, Nanosilver-based antibacterial drugs and devices: mechanisms, methodological drawbacks, and guidelines, *Chem. Soc. Rev.* 43 (5) (2014) 1501–1518.
- [28] Q.L. Feng, J. Wu, G.Q. Chen, F.Z. Cui, T.N. Kim, J.O. Kim, A mechanistic study of the antibacterial effect of silver ions on *Escherichia coli* and *Staphylococcus aureus*, *J. Biomed. Mater. Res.* 52 (4) (2000) 662–668.
- [29] S.L. Percival, P.G. Bowler, D. Russell, Bacterial resistance to silver in wound care, *J. Hosp. Infect.* 60 (1) (2005) 1–7.
- [30] M. Yamanaka, K. Hara, J. Kudo, Bactericidal actions of a silver ion solution on *Escherichia coli*, studied by energy-filtering transmission electron microscopy and proteomic analysis, *Appl. Environ. Microbiol.* 71 (11) (2005) 7589–7593.
- [31] P.L. Tran, E. Huynh, A.N. Hamood, A. de Souza, D. Mehta, K.W. Moeller, C. D. Moeller, M. Morgan, T.W. Reid, The ability of a colloidal silver gel wound dressing to kill bacteria in vitro and in vivo, *J. Wound Care* 26 (sup4) (2017) S16–S24.
- [32] M. Ueno, H. Miyamoto, M. Tsukamoto, S. Eto, I. Noda, T. Shobuie, T. Kobatake, M. Sonohata, M. Mawatari, Silver-containing hydroxyapatite coating reduces biofilm formation by methicillin-resistant *Staphylococcus aureus* in vitro and in vivo, *BioMed Res. Int.* 2016 (2016), 8070597.
- [33] R.J. Holmila, S.A. Vance, S.B. King, A.W. Tsang, R. Singh, C.M. Furdul, Silver nanoparticles induce mitochondrial protein oxidation in lung cells impacting cell cycle and proliferation, *Antioxidants* 8 (11) (2019).
- [34] D. Wang, M. Dan, Y. Ji, X. Wu, X. Wang, H. Wen, Roles of ROS and cell cycle arrest in the genotoxicity induced by gold nanorod core/silver shell nanostructure, *Nanoscale Res. Lett.* 15 (1) (2020) 224.
- [35] S. Takeshita, K. Kaji, A. Kudo, Identification and characterization of the new osteoclast progenitor with macrophage phenotypes being able to differentiate into mature osteoclasts, *J. Bone Miner. Res.* 15 (8) (2000) 1477–1488.
- [36] G.K. Mannala, M. Rupp, F. Alagboso, M. Kerschbaum, C. Pfeifer, U. Sommer, M. Kampschulte, E. Domann, V. Alt, *Galleria mellonella* as an alternative in vivo model to study bacterial biofilms on stainless steel and titanium implants, *ALTEX* 38 (2) (2021) 245–252.
- [37] M.A. Getzlaf, E.A. Lewallen, H.M. Kremers, D.L. Jones, C.A. Bonin, A. Dudakovic, R. Thaler, R.C. Cohen, D.G. Lewallen, A.J. van Wijnen, Multi-disciplinary antimicrobial strategies for improving orthopaedic implants to prevent prosthetic joint infections in hip and knee, *J. Orthop. Res.* 34 (2) (2016) 177–186.
- [38] C.L. Romano, S. Scarponi, E. Gallazzi, D. Romano, L. Drago, Antibacterial coating of implants in orthopaedics and trauma: a classification proposal in an evolving panorama, *J. Orthop. Surg. Res.* 10 (2015) 157.
- [39] S. Ferraris, S. Spriano, Antibacterial titanium surfaces for medical implants, *Mater. Sci. Eng., C Mater. Biol. Appl.* 61 (2016) 965–978.
- [40] G. Gosheger, J. Hardes, H. Ahrens, A. Streitburger, H. Buerger, M. Erren, A. Gunsel, F.H. Kemper, W. Winkelmann, C. Von Eiff, Silver-coated megaendoprostheses in a rabbit model—an analysis of the infection rate and toxicological side effects, *Biomaterials* 25 (24) (2004) 5547–5556.
- [41] A. Wilke, G. Schroder, J. Orth, P. Griss, R.P. Franke, [Evaluation of the biocompatibility of implant materials with human bone marrow cell cultures], *Biomed. Tech.* 38 (6) (1993) 126–129.
- [42] S. Ferraris, A. Venturello, M. Miola, A. Cochis, L. Rimondini, S. Spriano, Antibacterial and bioactive nanostructured titanium surfaces for bone integration, *Appl. Surf. Sci.* 311 (2014) 279–291.
- [43] Y. Kirmanidou, M. Sidira, A. Bakopoulou, A. Tsouknidas, O. Prymak, R. Papi, T. Choli-Papadopoulou, M. Epple, N. Michailidis, P. Koidis, et al., Assessment of cytotoxicity and antibacterial effects of silver nanoparticle-doped titanium alloy surfaces, *Dent. Mater.* 35 (9) (2019) E220–E233.
- [44] S. Sandukas, A. Yamamoto, A. Rabiei, Osteoblast adhesion to functionally graded hydroxyapatite coatings doped with silver, *J. Biomed. Mater. Res.* 97 (4) (2011) 490–497.
- [45] A. Rodriguez-Contreras, D. Torres, B. Rafik, M. Ortiz-Hernandez, M.P. Ginebra, J. A. Calero, J.M. Manero, E. Ruperez, Bioactivity and antibacterial properties of calcium- and silver-doped coatings on 3D printed titanium scaffolds, *Surf. Coating. Technol.* (2021) 421.
- [46] J. Jaishankar, P. Srivastava, Molecular basis of stationary phase survival and applications, *Front. Microbiol.* 8 (2017) 2000.
- [47] T. Abdulrehman, S. Qadri, S. Skariah, A. Sultan, S. Mansour, J. Azzi, Y. Haik, Boron doped silver-copper alloy nanoparticle targeting intracellular *S. aureus* in bone cells, *PLoS One* 15 (4) (2020), e0231276.
- [48] L. Pauksch, S. Hartmann, M. Rohnke, G. Szalay, V. Alt, R. Schnettler, K.S. Lips, Biocompatibility of silver nanoparticles and silver ions in primary human mesenchymal stem cells and osteoblasts, *Acta Biomater.* 10 (1) (2014) 439–449.
- [49] M. Esposito, L. Murray-Curtis, M.G. Grusovin, P. Coulthard, H.V. Worthington, Interventions for replacing missing teeth: different types of dental implants, *Cochrane Database Syst. Rev.* 4 (2007), Cd003815.
- [50] E.P. Ivanova, V.K. Truong, J.Y. Wang, C.C. Berndt, R.T. Jones, Yusuf II, I. Peake, H. W. Schmidt, C. Fluke, D. Barnes, et al., Impact of nanoscale roughness of titanium thin film surfaces on bacterial retention, *Langmuir* 26 (3) (2010) 1973–1982.
- [51] E. Medilanski, K. Kaufmann, L.Y. Wick, O. Wanner, H. Harms, Influence of the surface topography of stainless steel on bacterial adhesion, *Biofouling* 18 (3) (2002) 193–203.
- [52] E.A. Seiss, A. Krone, P. Formaglio, O. Goldmann, S. Engelmann, B. Schraven, E. Medina, A.J. Muller, Longitudinal proliferation mapping in vivo reveals NADPH oxidase-mediated dampening of *Staphylococcus aureus* growth rates within neutrophils, *Sci. Rep.* 9 (1) (2019) 5703.
- [53] N. Ciacotich, M. Kilstrup, P. Moller, L. Gram, Influence of chlorides and phosphates on the antiadhesive, antibacterial, and electrochemical properties of an electroplated copper-silver alloy, *Biointerphases* 14 (2) (2019), 021005.
- [54] E. Zielinska, C. Tukaj, M.W. Radomski, I. Inkielewicz-Stepniak, Molecular mechanism of silver nanoparticles-induced human osteoblast cell death: protective effect of inducible nitric oxide synthase inhibitor, *PLoS One* 11 (10) (2016), e0164137.
- [55] J. Hardes, A. Streitburger, H. Ahrens, T. Nusselt, C. Gebert, W. Winkelmann, A. Battmann, G. Gosheger, The influence of elementary silver versus titanium on osteoblasts behaviour in vitro using human osteosarcoma cell lines, *Sarcoma* 2007 (2007), 26539.
- [56] S.E. Taylor, M. Shah, I.R. Orriss, Generation of rodent and human osteoblasts, *BoneKey Rep.* 3 (2014) 585.
- [57] M. Ahmad, M.B. McCarthy, G. Gronowicz, An in vitro model for mineralization of human osteoblast-like cells on implant materials, *Biomaterials* 20 (3) (1999) 211–220.
- [58] H. Cao, Y. Qiao, X. Liu, T. Lu, T. Cui, F. Meng, P.K. Chu, Electron storage mediated dark antibacterial action of bound silver nanoparticles: smaller is not always better, *Acta Biomater.* 9 (2) (2013) 5100–5110.
- [59] A. Gao, R. Hang, X. Huang, L. Zhao, X. Zhang, L. Wang, B. Tang, S. Ma, P.K. Chu, The effects of titania nanotubes with embedded silver oxide nanoparticles on bacteria and osteoblasts, *Biomaterials* 35 (13) (2014) 4223–4235.
- [60] R.E. Hall, G. Bender, R.E. Marquis, In vitro effects of low intensity direct current generated silver on eukaryotic cells, *J. Oral Maxillofac. Surg.* 46 (2) (1988) 128–133.
- [61] E.S. Pshennikova, S.Y. Filippovich, G.P. Bachurina, V.D. Ponomareva, A. G. Malygin, [The different effects of carbon dioxide on the toxicity of silver ions for prokaryotic and eukaryotic microorganisms], *Izv. Akad. Nauk Ser. Biol. (Mosc.)* (3) (2011) 354–357.
- [62] D. Lee, W.K. Ko, S.J. Kim, I.B. Han, J.B. Hong, S.H. Sheen, S. Sohn, Inhibitory effects of gold and silver nanoparticles on the differentiation into osteoclasts in vitro, *Pharmaceutics* 13 (4) (2021).
- [63] L. Pauksch, M. Rohnke, R. Schnettler, K.S. Lips, Silver nanoparticles do not alter human osteoclastogenesis but induce cellular uptake, *Toxicol Rep* 1 (2014) 900–908.
- [64] G. Menard, A. Rouillon, V. Cattoir, P.Y. Donnio, *Galleria mellonella* as a suitable model of bacterial infection: past, present and future, *Front. Cell. Infect. Microbiol.* 11 (2021), 782733.